ECcentric Circle ENcoding TRajectorIes for Compressed-sensing (ECCENTRIC): A fully random non-Cartesian sparse Fourier domain sampling for MRSI at 7 Tesla

Antoine Klauser[a,b,g] , Bernhard Strasser[b,c] , Wolfgang Bogner[c] ,Lukas Hingerl[c] ,Claudiu Schirda[d], Bijaya Thapa[b], Daniel Cahill[e], Tracy Batchelor[f], Francois Lazeyras[a,g], Ovidiu Andronesi[b]

[a]Department of Radiology and Medical Informatics, University of Geneva, Switzerland

[b] Athinoula A. Martinos Center for Biomedical Imaging, Department of Radiology, Massachusetts General Hospital, Harvard Medical School, Boston

[c]High-Field MR Center, Department of Biomedical Imaging and Image-guided Therapy, Medical University of Vienna, Vienna, Austria

[d]Department of Radiology, University of Pittsburgh School of Medicine,Pittsburgh, Pennsylvania, USA

[e]Department of Neurosurgery, Massachusetts General Hospital, Harvard Medical School, Boston

[f]Department of Neurology, Brigham and Women, Harvard Medical School, Boston

[g]CIBM Center for Biomedical Imaging, Switzerland

Synposis (max 100 words):

A new encoding trajectory for magnetic resonance spectroscopic imaging was developed and implemented on a 7T human scanner. ECcentric Circle ENcoding TRajectorIes for Compressed-sensing (ECCENTRIC) is a spatial-spectral encoding strategy optimized for random non-Cartesian sparse Fourier domain sampling. Acceleration by undersampling ECCENTRIC prevents coherent aliasing artefacts in the spatial response function. ECCENTRIC allows smaller circles to avoid temporal interleaving for large matrix size, which is beneficial for spectral quality. Circle trajectories need limited gradient slewrate without rewinding deadtime,and are robust to timing imperfection and eddy-current delays.

Introduction:

A major drawback of MRSI is long acquisition times for 4D (k,t) spatio-temporal space, resulting in critical need for high acceleration strategies. This is particularly relevant for high-resolution whole-brain MRSI where traditional acquisition schemes require several hours. Acceleration can be performed by parallel imaging such as SENSE and GRAPPA with uniform undersampling, or by Compressed-Sensing (CS) with random undersampling, but these techniques generally don't allow acceleration factors (AF) above 10[1,2]. Spatial-spectral encoding (SSE) techniques enable higher AF of 10-100[3], but current SSE trajectories require temporal interleaves at ultra-high field to reach a broad spectral bandwidth and high spatial resolution. However, temporal interleaving creates spectral sidebands that reduce SNR and overlap with metabolite signals. Thus, it should be avoided[3]. Circular waveforms are characterized by absence of deadtime for repeated rewinding, and have constant and moderate gradient slewrate not demanding for gradient hardware.

We introduce ECCENTRIC, a novel SSE trajectory following a random pattern of off-center circles weighted with a highly desired 1/|k| density function particularly suitable for sparse undersampling acceleration to prevent coherent aliasing artefacts. With this approach the circle size can be chosen to prevent the use of temporal interleaving independently of the spatial resolution.

Method:

ECCENTRIC Trajectory

The 3D k-space is divided into a stack of k_x-k_y planes where off-center circles are measured, while k_z is encoded by Cartesian phase-encoding. The number of eccentric circles necessary to achieve full sampling k_x-k_y planes is derived from one type of rosette trajectory that needs[4] n*pi/2 circles with n being the matrix size. The number of circles of radius r for full sampling is given by $n*pi*k_{xy}^{max}/(2*r)$ with k_{xy}^{max} the largest in-plane k-space absolute value (FIG.1). To achieve spherical 3D k-space coverage, k_{xy}^{max} is decreased along the 3rd dimension following $k_{xy}^{max}=n/(2*FoV)*sqrt(1-(k_z/k_z^{max})^2)$. A short constant-time gradient ramp is used to reach initial off-center k_{xy} position and velocity, which is applied simultaneously with the excitation rewinder and phase encoding (Fig.1). Circle center positions, parametrized by polar coordinates (r_c,phi_c) (FIG.1), are chosen randomly and differently for each plane with r_c in [0,max(k^{max}-r,r)] and phi_c in [0,2*pi]. The homogeneous distribution of points in polar coordinates results in 1/|k| weighting in the Cartesian k-space.

Spatial response function[5] (SRF) was obtained for impulse data of a point source and 64x64 matrix reconstructed with NUFFT[6] for ECCENTRIC, rosette and concentric circle trajectories.

Sequence and acquisition parameters

The ECCENTRIC was implemented on a 7T scanner (Terra/Siemens/Erlangen/Germany) with a NOVA head coil (32Rx/8Tx) and appended to a FID-MRSI sequence[7] with 0.9ms echo-time (TE), 35° excitation flip-angle and 450ms repetition-time (TR) and WET water suppression. The Field-of-View (FoV) was set to (A/P-R/L-H/F) 220x220x45mm^3 with 35mm-thick excited slab. The spatial resolution was 64x64x9 resulting in a 3.4x3.4x5mm^3 voxel size. The ECCENTRIC circle radius was set to 64/(8*FoV) (half the rosette circle radius), the spectral bandwidth set to 2326Hz didn't require temporal interleaving, and the FID was sampled for 350ms. The resulting acquisition time of fully sampled data was 8min. Water reference was acquired with the same sequence but smaller matrix size (22x22x7) in 2min.

Reconstruction and metabolite quantification

The non-Cartesian MRSI signal was reconstructed into image space using the Total-Generalized-Variation (TGV) constrained low-rank model9,10,11
allowing for reconstruction of randomly undersampled k-space. Assuming that the magnetization can be separated into a

$$\rho(\mathbf{r},t)=\sum_{n=1}^{K}U_n(\mathbf{r})V_n(t)$$

small number of spatial and temporal components

, these components are retrived by the minimization problem

$$\arg\min_{\mathbf{UV}}\|\mathbf{s}-\mathcal{FCB}\mathbf{UV}\|_2^2+\lambda\sum_{n=1}^{K}\mathrm{TGV}^2\{U_n\}$$

with s the measured data, F, the encoding operator,
C, the coil sensitivity operator, B, the frequency shift operator and lambda is the TGV regularization parameter.

The reconstruction was preceded by skull-lipid suppression by spectral orthogonality [8,10]. The reconstructed MRSI dataset was quantified using LCModel[12].

Experimental tests

ECCENTRIC FID-MRSI data were acquired on a high resolution structural-metabolic phantom, two healthy volunteers and a brain tumor patient. Acceleration performance was assessed by retrospective undersampling of the trajectory and compared to fully sampled data by peak-SNR and SSIM of metabolic maps, and FWHM, CRLB, and SNR obtained from LCModel.

Results:

In Fig.2, we show the incoherent aliasing in SRF of undersampled ECCENTRIC and the SRF pattern is conserved for different AF. In comparison, rosette and concentric circles tend to create more coherent pattern when trajectories are undersampled, and their SRF changes with AF. This indicates that ECCENTRIC is more suitable for acceleration by Compressed-Sensing than these trajectories. The high-resolution phantom illustrates the capability to resolve a range of structural features up to the acquired spatial resolution of 3.4mm.

Reconstructed metabolite maps from a healthy volunteer are shown in Fig.3. The grey-white matter contrast particularly present in the Glx map indicates the sensitivity of the method for the lower signal of J-coupled metabolites. Spectral quality does not decrease strongly with acceleration.

In Fig.4, brain tumor patient data are shown for Cho, tNAA and Cho/tNAA ratio maps. The tumor is clearly visible for all AF, although for AF=3 some areas of the healthy brain present more noise. Spectra show similar metabolic profiles for all AF, albeit a slight increase of noise. The apparent higher noise in patient data is due to a titanium plate and screws after brain surgery, which downgrades B_0 and B_1 homogeneity.

Discussion:

We presented a new trajectory: ECCENTRIC that enables the acquisition of high-resolution MRSI without temporal interleaving and with random sparse sampling of the Fourier domain for unrestricted axial brain coverage, which has high potential for clinical applications. Work in progress explores higher spatial resolution and larger brain slab coverage with greater acceleration factors.

References:

[1] Strasser, B., Považan, M., Hangel, G., Hingerl, L., Chmelik, M., Gruber, S., … Bogner, W. (2017). Magnetic Resonance in Medicine, 78(2), 429–440.
[2] Nassirpour, S., Chang, P., Avdievitch, N., & Henning, A. (2018). Magnetic Resonance in Medicine, 80(6), 2311–2325.
[3] Bogner, W., Otazo, R., & Henning, A. (2020). NMR in Biomedicine, e4314.
[4] Schirda, C. V., Tanase, C., & Boada, F. E. (2009). Journal of Magnetic Resonance Imaging, 29(6), 1375–1385.
[5] Mareci, T. H., & Brooker, H. R. (1991). Journal of Magnetic Resonance (1969), 92(2), 229–246.
[6] Fessler JA, Sutton BP. IEEE Trans Signal Process 2003; 51:560–574.
[7] Henning, A., Fuchs, A., Murdoch, J. B., & Boesiger, P. (2009). NMR in Biomedicine, 22(7), 683–696.
[8] Bilgic, B., Gagoski, B., Kok, T. and Adalsteinsson, E. (2013). Magnetic Resonance in Medicine 69, 1501-1511
[9] Kasten, J., Lazeyras, F., & Van De Ville, D. (2013). IEEE Transactions On Medical Imaging, 32(10), 1853–1863.
[10] Klauser, A., Courvoisier, S., Kasten, J., Kocher, M., Guerquin-Kern, M., Van De Ville, D., & Lazeyras, F. (2019). Magnetic Resonance in Medicine, 81(5), 2841–2857.
[11] Klauser, A., Courvoisier, S., Kocher, M., Van De Ville, D., & Lazeyras, F. (2018). Whole Brain 5mm-isotropic 3D 1H-FID-MRSI accelerated with Compressed- Sensing SENSE. ISMRM annual meeting proceeding #3847
[12] Provencher, S.W. (1993). Magnetic Resonance in Medicine *30*, 672-679.

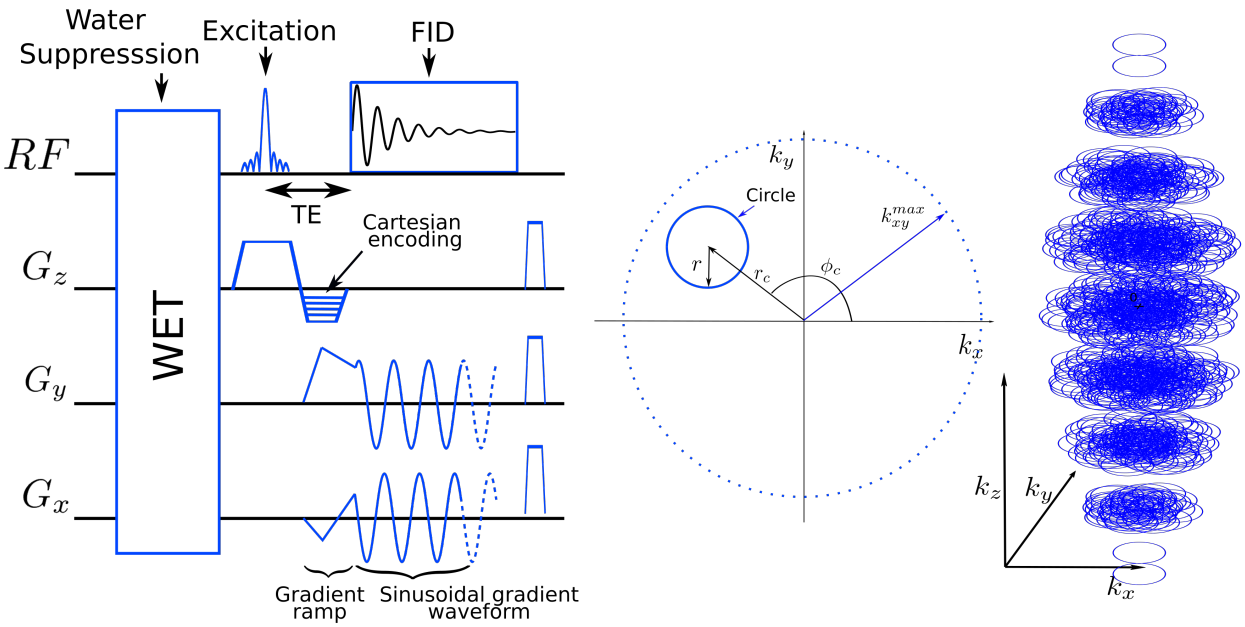

Figure 1: Sketch of the FID-ECCENTRIC sequence. 4-pulses WET water suppression precedes the excitation pulse. After the excitation, cartesian encoding along z-axis and gradient ramp along x and y axes are played before the acquisition simultaneous to the sinusoidal gradient waveform. Right, the parametrization of the circle position and the Fourier domain trajectory of ECCENTRIC for a 64x64x9 encoding matrix.

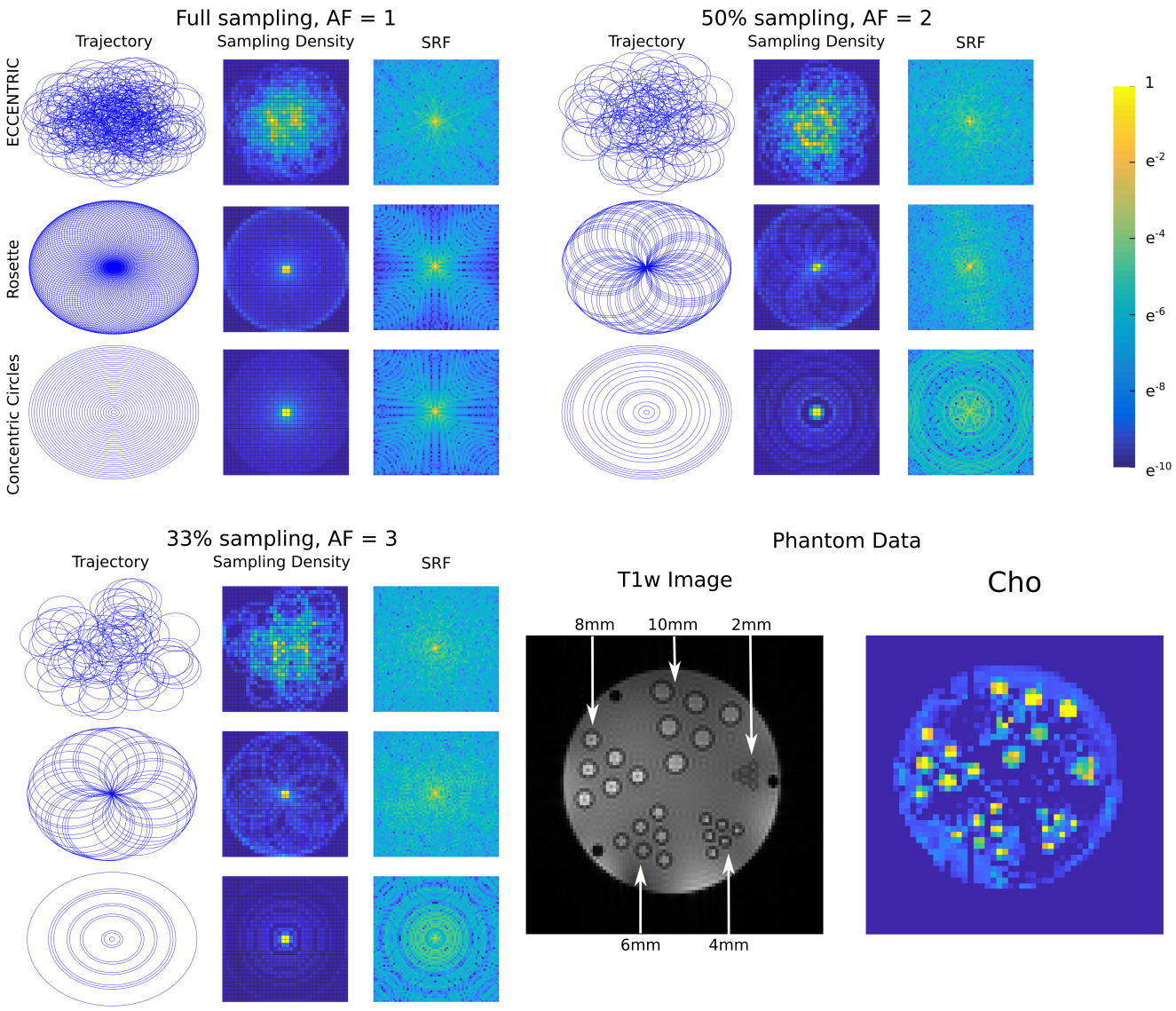

Figure 2: Comparison of the ECCENTRIC, rosette and concentric circles trajectories for AFs = 1,2,3. The sampling trajectories and the sampling density are shown in the k-space, and the spatial response function (SRF) were computed with or without random undersampling. Although ECCENTRIC results in larger signal leakage in the neighbouring voxels, especially at full sampling, it is more randomly distributed (noise-like) in comparison to the more structured artefacts such as ripples and ringing observed in rosette and concentric circles. Also the general aspect of SRF for ECCENTRIC seems to be conserved over different AF, while SRF changes with AF for rosettes and concentric circles. Bottom right, the Choline (Cho) map resulting from ECCENTRIC FID-MRSI acquisition on the high-resolution phantom is presented. Cho containing tubes of diameters down to 4mm can be resolved in agreement with the in-plane sequence spatial resolution (3.4x3.4mm).

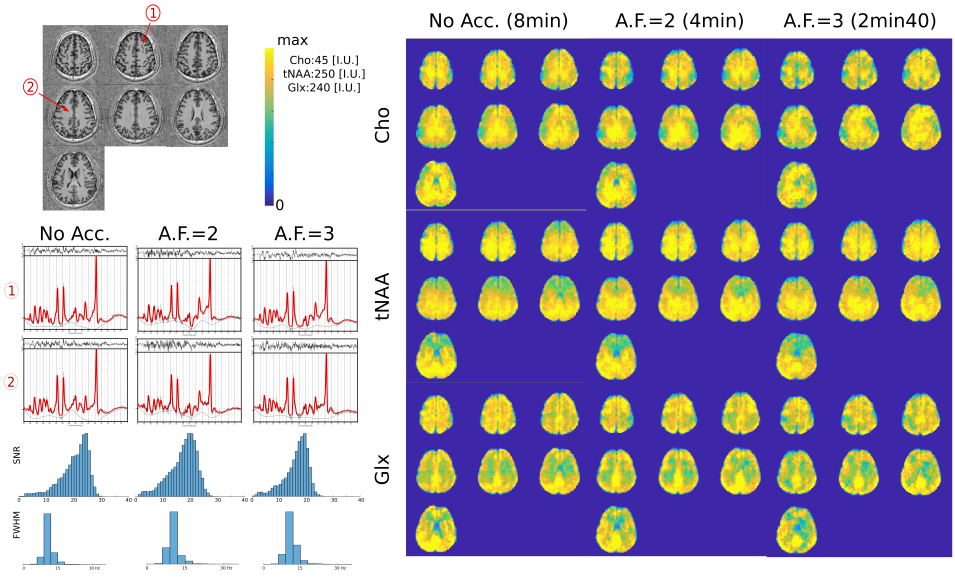

Figure 3. Healthy volunteer metabolite maps acquired with ECCENTRIC FID-MRSI and accelerated retrospectively. Right: maps of Choline (Cho), total NAA (tNAA) and Glutamate+Glutamine (Glx) are shown for no acceleration, acceleration factor 2 and 3. Left: two sample spectra from the frontal and central region are displayed. Histograms show the distribution of Signal-to-Noise (SNR) and full-width-at-half-maximum (FWHM) in the voxels of the slab.

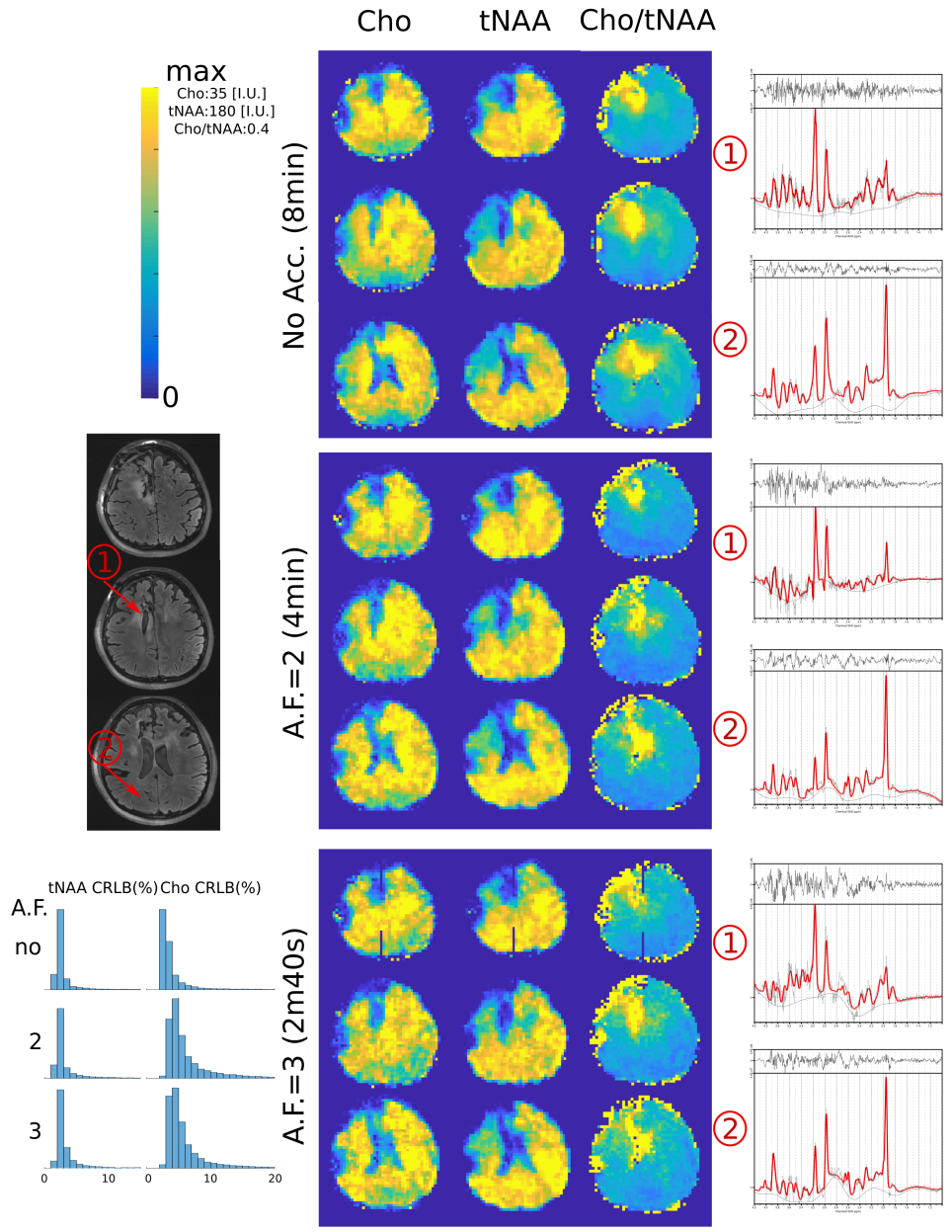

Figure 4: Choline (Cho), total NAA (tNAA) and ratio maps resulting from ECCENTRIC FID-MRSI acquisition performed on a brain tumor patient. Results from retrospective acceleration AF=2 and AF=3 show that the tumor lesion and contrast was preserved through acceleration. Spectra from the tumor location (1) and healthy tissue (2) are shown for all AFs. Bottom left, histograms of the Cramer-Rao Lower Bound (CRLB) for tNAA and Cho LCModel fit from the entire slab are presented.